UDC 550.388.2

# Numerical modeling of the electron density enhancements in the night-time ionospheric F2-layer

**M.A. Knyazeva, Yu.V. Romanovskaya, A.A. Namgaladze**
*Polytechnic Faculty of MSTU, Physics Department*

**Abstract.** The middle-latitude enhanced electron density regions (EEDRs) in the night-time ionospheric F2-layer have been investigated using the global numerical Upper Atmosphere Model (UAM) and the empirical ionospheric model IRI-2001. The mechanism of formation, seasonal and latitudinal-longitudinal variations of the EEDRs has been studied. It has been shown that two types of the EEDRs exist on the geomagnetic foF2 maps: 1) winter type with maxima in the latitudinal and diurnal foF2 variations and 2) summer type with the maximum in the latitudinal variation only. Formation of both types of the EEDRs is explained by the corresponding seasonal variations of the thermospheric wind. The physical mechanism of the EEDRs forming is based on the joint action of the plasma flows from the plasmasphere and the neutral wind inducing transportation of the ionospheric plasma along the geomagnetic field lines. The Weddell Sea Anomaly and the analogous phenomenon observed in the Northern Hemisphere have been explained.

**Аннотация.** С помощью глобальной численной модели верхней атмосферы Земли (UAM) и эмпирической модели ионосферы IRI-2001 исследуются ночные среднеширотные области повышенной электронной концентрации (ОПЭК) в ионосферном F2-слое. Обсуждаются механизм формирования, сезонные и долготные вариации ОПЭК. На основе анализа геомагнитных карт широтно-долготных вариаций foF2 показано существование двух типов ОПЭК: 1) зимний тип с максимумами в широтной и суточной вариациях foF2 и 2) летний тип с максимумом только в широтной вариации. Формирование обоих типов ОПЭК объясняется соответствующими сезонными вариациями термосферного ветра. Физический механизм формирования ОПЭК основан на совместном действии потоков плазмы из плазмосферы и переноса ионосферной плазмы вдоль геомагнитных силовых линий нейтральным ветром. В работе также обсуждаются аномалия моря Уэдделла и аналогичный феномен, наблюдаемый в северном полушарии.

**Key words:** ionosphere, thermospheric wind, thermosphere-ionosphere coupling, electromagnetic drift, Weddell Sea Anomaly, numerical modeling
**Ключевые слова:** ионосфера, термосферный ветер, термосферно-ионосферное взаимодействие, электромагнитный дрейф, аномалия моря Уэдделла, численное моделирование

## 1. Introduction

The anomalous night-time enhancements of the electron density in the middle-latitude ionospheric $F_2$-layer were first described by *Gilliland* (1935). Further numerous observations had shown that the analogous enhancements of the plasma density at the F2-layer altitudes are manifested as the pre-midnight and/or post-midnight maxima in the diurnal and latitudinal variations of the F2-layer critical frequency (foF2) and maximal electron density (NmF2), total electron content in unit section column (TEC) (*Evans*, 1965; *Da Rosa, Smith*, 1967; *Klobuchar et al.*, 1968; *Titheridge*, 1968; 1973; *Bertin, Lepine*, 1970; *Young et al.*, 1970; *Park*, 1971; *Davies et al.*, 1979; *Rao et al.*, 1982; *Balan et al.*, 1986; 1991; *Balan, Rao*, 1987; *Joshi, Iyer*, 1990; *Jakowski et al.*, 1991; *Richards et al.*, 1994; 2000; *Horvath, Essex*, 2000; *Mikhailov et al.*, 2000; *Farelo et al.*, 2002).

The reconstruction of the global TEC maps obtained from the GPS satellite network allowed estimating two-dimensional (latitudinal-longitudinal and latitudinal-temporal) TEC variations. On global maps these night-time enhancements are clearly visible in the form of the enhanced electron density regions (EEDRs) at the geomagnetic middle-latitudes 25°-45° (*Wilson et al.*, 1995; *Davies, Hartmann*, 1997; *Ho et al.*, 1996; 1998; *Brunini et al.*, 2003). The EEDRs extend from evening sector to morning one.

The EEDRs are observed more often in the quiet winter conditions under low solar activity (*Balan et al.*, 1991; *Garner et al.*, 1994; *Mikhailov et al.*, 2000; *Farelo et al.*, 2002).

Some authors consider that the cause of the EEDRs formation is related mainly to the ion transportation by the eastward electric field induced $\boldsymbol{E}\times\boldsymbol{B}$ drift. The ionospheric plasma drifts to lower geomagnetic latitudes where the geomagnetic force tubes have smaller volumes (*Park*, 1971; *Evans*, 1965; *Davies et al.*, 1979; *Balan, Rao*, 1987; *Förster, Jakowski*, 1988; *Balan et al.*, 1991; *Jakowski, Förster*, 1995; *Horvath, Essex*, 2000). The tubes are compressed and it results in the EEDRs formation. In the night sector the equatorward neutral wind

contributes to EEDRs forming (*Bailey et al.*, 1991; *Pavlov, Pavlova*, 2005). The wind drives the F2-layer plasma to higher altitudes at which the ion loss rate is lower. However, *Richards et al*. (2000) used Millstone Hill radar measurements of densities, temperatures, and drift velocities to show that the measured $\boldsymbol{E}\times\boldsymbol{B}$ drifts do not cause the large nighttime enhancements. They attributed the anomalous density enhancements to the electron temperature, which remained high between sunset and midnight and then dropped precipitously causing a large downward ionization flux.

However, the equatorward electromagnetic drift of the plasma moves the F2-layer downward to altitudes where the ion $O^+$ loss rate is larger, thus decreasing NmF2.

Besides the described EEDRs the observations demonstrate other events of the night-time F2-layer electron density enhancements: the Weddell Sea Anomaly in the Southern Hemisphere (*Bellchambers, Piggot*, 1958; *Penndorf*, 1965) and the analogous phenomenon in the Northern Hemisphere (*Thampi et al.*, 2009).

The Weddell Sea Anomaly (WSA) is anomalous because the nighttime F2-layer electron densities exceed the daytime densities in the Antarctic region from 40°S to 80°S geodetic latitude and about 255°-315° geodetic longitude (*Horvath, Essex*, 2003; *Horvath*, 2006; *Burns et al.*, 2008; *Lin et al.*, 2009; *He et al.*, 2009; *Horvath, Lovell*, 2009a,b,c; 2010; *Jee et al.*, 2009; *Karpachev et al.*, 2010; *Liu et al.*, 2010). The WSA is formed in the summer solstice under quiet geomagnetic conditions and low solar activity.

The analogous phenomenon takes place in the Northern summer Hemisphere from about 40°N to 80°N in latitude at the meridians of 75°-135° in longitude. Neither phenomena have been observed in winter.

Numerous papers discussed the mechanisms including the joined effects of solar ionization and thermospheric winds (*Dudeney, Piggott*, 1978; *Horvath*, 2006; *Liu et al.*, 2010), geomagnetic field geometry (*Horvath, Essex*, 2003; *Horvath*, 2006), non-coincidence of the geomagnetic and geodetic axes (*Lin et al.*, 2009), downward plasma fluxes from the plasmasphere (*Burns et al.*, 2008), energetic particle precipitation (*Pavlov, Pavlova*, 2007), electric fields (*Burns et al.*, 2008; *Horvath, Lowell*, 2009b) and plasma convection effects (*Penndorf*, 1965). Some authors consider that the principal role in the anomalies formation belongs to neutral winds (*Horvath*, 2006; *He et al.*, 2009; *Karpachev et al.*, 2010).

All hypotheses of the EEDRs forming are only qualitative and require the quantitative estimation of each plasma transfer process contribution in the electron density distribution in the night-time middle-latitude F2-layer. This approach is realized by means of the mathematical modeling method.

This paper is devoted to numerical modeling of the electron density enhancements in the night-time ionospheric F2-layer by using the numerical Upper Atmosphere Model (UAM). Our investigation is not a case-study but an attempt to reproduce the EEDRs in a frame of a global ionospheric spatial and temporal structure as its parts. We compare our UAM calculation results with predictions of the well known and widely used empirical IRI-2001 model (*Bilitza*, 2001) providing global distribution of ionospheric parameters such as NmF2 and hmF2.

## 2. Global numerical Earth's Upper Atmosphere Model (UAM)

The Upper Atmosphere Model is a global, three-dimensional, time-dependent, numerical model simulating the thermosphere, ionosphere, plasmasphere and inner magnetosphere of the Earth as a single system. It was initially developed at the Kaliningrad observatory (now West Department) of IZMIRAN (*Namgaladze et al*., 1988; 1991) and then extended at the Polar Geophysical Institute of the Russian Academy of Sciences and at the Murmansk State Technical University (*Namgaladze et al.*, 1998). The model includes the equations of the continuity, momentum and heat balance and the electric potential equation and calculates the concentrations, velocity vectors and temperatures of basic neutral ($O_2$, $N_2$, O) and charged ($NO^+$, $O_2^+$, $O^+$, $H^+$ and $e$) components of the atmosphere at the altitude range from 60 km to 100000 km.

The following continuity equations are solved in the model:

$$\partial n_\alpha/\partial t + \nabla(n_\alpha \boldsymbol{V}_\alpha) = Q_\alpha - L_\alpha,\ \alpha = n, i, e, \tag{1}$$

where the subscripts $n$, $i$ and $e$ refer to neutral components, ions and electrons, respectively; $n_\alpha$, $Q_\alpha$, $L_\alpha$ are the concentration, the production and loss rates of $\alpha$-gas, respectively; $\mathbf{V}_\alpha$ is the weight-average velocity vector of $\alpha$-gas.

The following momentum equations are solved in the model:

$$\rho_\alpha[d\boldsymbol{V}_\alpha/dt + \boldsymbol{\Omega}\times(\boldsymbol{\Omega}\times\boldsymbol{r}) + 2\boldsymbol{\Omega}\times\boldsymbol{V}_\alpha] = \boldsymbol{F}_\alpha, \tag{2}$$

where $\boldsymbol{\Omega}$ is the Earth's angular velocity vector; $\boldsymbol{r}$ is the radius-vector from the Earth's centre; $\rho_\alpha$ is the mass density of $\alpha$-gas; $\boldsymbol{F}_\alpha$ is the force acting on $\alpha$-gas volume unit.

The following heat balance equations are solved in the model:

$$\rho_\alpha c_{v\alpha} dT_\alpha/dt + p_\alpha \nabla\boldsymbol{V}_\alpha = \nabla(\lambda_\alpha \nabla T_\alpha) + P_{Q\alpha} - P_{L\alpha} + P_{T\alpha}, \tag{3}$$

where $c_{v\alpha}$ is the specific heat at constant volume of $\alpha$-gas; $\lambda_\alpha$ is the thermal conductivity coefficient of $\alpha$-gas; $T_\alpha$ is $\alpha$-gas temperature; $p_\alpha$ is $\alpha$-gas pressure; $P_{Q\alpha}$, $P_{L\alpha}$ are the rates of heating and heat loss of $\alpha$-gas; $P_{T\alpha}$ – the rate of the elastic and inelastic exchange of heat between $\alpha$-gas and other gases.

The equation for the potential $\varphi$ of the electric field $\boldsymbol{E} = -\nabla\varphi$ is solved numerically taking into account the dynamo-action of the thermospheric winds:

$$\nabla [\sigma (\nabla\varphi - \boldsymbol{V}\times\boldsymbol{B}) - \boldsymbol{j_m}] = 0, \quad (4)$$

where $\sigma$ is the ionospheric conductivity tensor; $\boldsymbol{V}$ is the neutral wind velocity vector; $\boldsymbol{B}$ is the magnetic field; $\boldsymbol{j_m}$ is the magnetospheric current density.

The equations (1-3) take into account the photodissociation of molecular oxygen, photoionization by the direct and scattered solar radiation and corpuscular ionization of neutral components, ion-molecular reactions, dissociative recombination of molecular ions, charge exchange reactions and transfer processes (ambipolar diffusion, ion drag, ion-ion friction and electromagnetic drift) for atomic ions, neutral gas pressure gradients, molecular and turbulent diffusions, neutral-ion and viscous frictions, heating by UV and EUV solar radiation, Joule heating and heating by precipitating energetic particles, heat conductivity, heating of neutral gas due to chemical reactions and heat losses due to radiation.

The system of equations (1-4) is completed by initial and boundary conditions.

At the upper boundary ($h$ = 520 km) of the model neutral atmosphere we assume that:

$$\partial\boldsymbol{V}/\partial r = \partial T/\partial r = 0, \quad (5)$$

and all neutral components are in the diffusion equilibrium there. At the lower boundary ($h$ = 60 km) the wind velocity is taken according to the geostrophical approximation and the neutral temperature and densities are taken from the NRLMSISE-00 empirical thermospheric model (*Picone et al.*, 2002). The neutral atmosphere parameters and electric field potential are calculated in the spherical geomagnetic coordinate system.

The neutral atmosphere parameters are interpolated to the nodes of the finite-difference magnetic dipole coordinate grid to calculate the parameters of the ionospheric F2 region and plasmasphere taking into account electromagnetic plasma drift perpendicular to geomagnetic field lines. The boundary conditions for the model ionosphere are given near the base of the field lines in the Northern and Southern Hemispheres at height of 175 km. The atomic ion densities at this boundary are obtained from photochemical equilibrium conditions. The values of the ion and electron temperatures at this boundary are calculated from the equations of heat balance. We assume that geomagnetic field lines with $L \geq 15$ ($L$ parameter of McIlwain) are open and ion densities and heat fluxes are set equal to zero at the altitude of $15R_E$, where $R_E$ is the Earth radius.

Initial conditions are the stationary solution of the modelling equation system. To obtain this solution we integrate equations (1-4) until the results of integration do not differ under continuating of integration.

The detailed expressions for all coefficients and terms of the equations (1-4) can be found in (*Namgaladze et al.*, 1988; *Brunelli, Namgaladze*, 1988).

The UAM takes into account the non-coincidence of the geodetic and geomagnetic axes and gives the opportunity to model upper atmosphere parameters variations with the coincided axes. Besides the fully self-consistent version the model can be configured alternatively using empirical models, for example, the model of neutral composition and temperatures NRLMSISE-00 and the empirical horizontal wind model HWM-93 (*Hedin et al.*, 1996) as the corresponding model parts.

**3. EEDRs forming mechanism**

For estimating the relative role of the thermosphere wind and electric field in the EEDRs forming we analyzed the electron density time and spatial variations obtained by four UAM versions: 1) with ion drag induced by the thermospheric wind and the electromagnetic plasma drift (named by "version with wind and drift"); 2) with wind, but without drift; 3) without wind, but with drift and 4) without both wind and drift. The thermospheric parameters are calculated using the empirical thermospheric NRLMSISE-00 model (*Picone et al.*, 2002).

In the first and second versions of the model calculation ("with wind") thermospheric wind velocities are calculated using neutral gas pressure values obtained from the NRLMSISE-00 model. In the third and forth versions the thermospheric wind is equal to zero.

In the (1, 3) calculation versions ("with drift") the electric field distribution which determines electromagnetic drift velocities is calculated solving the equation for the electric potential (5) using the potential drop $\Delta\varphi$ across the polar cap (*Weimer et al.*, 1990) as the input parameter. In the second and forth versions electric field values are equal to zero.

The day 16.04.2002 represents quiet condition (near equinox). All model calculations use the same initial conditions which were obtained by several iterations of the model equations system integration for the same date

until the results of two next iterations become equal to each other (the stationary solution).

Fig. 1 presents the geomagnetic foF2 maps at the night longitudinal sector (18:00-06:00 MLT) calculated by all model versions for 24:00 UT. The midday-midnight geodetic meridian, the terminator and geodetic equator are drawn on the maps.

The night-time middle-latitude EEDRs (pointed by the black arrows) are more evident on foF2 maps obtained by versions with thermospheric winds (1, 2). The maps corresponding to the version without winds (3, 4) do not reveal these regions.

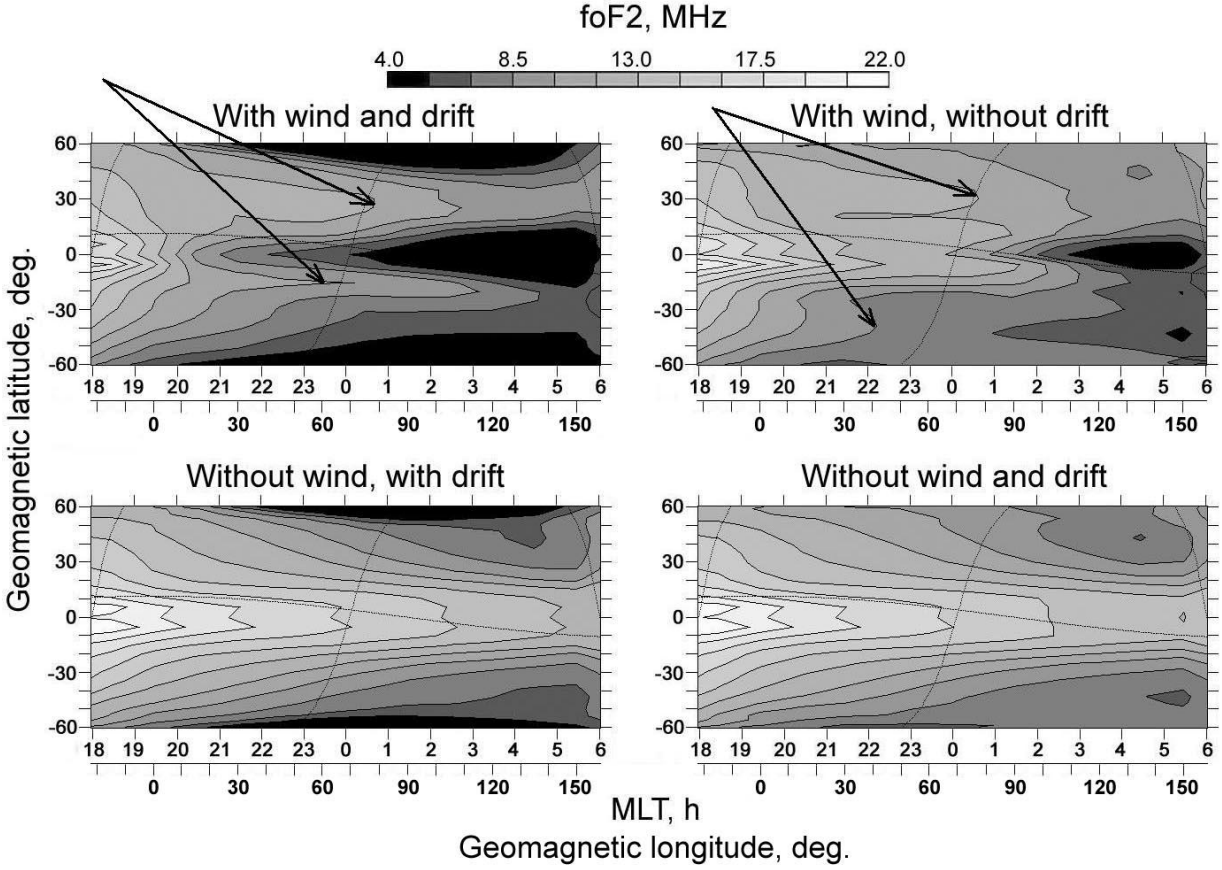


Fig. 1. Geomagnetic foF2 maps at the night longitudinal sector (18:00-06:00 MLT) calculated by the UAM-MSIS version for 24:00 UT 16.04.2002. The midday-midnight geodetic meridian, the terminator and geodetic equator are drawn by the dotted lines on the maps. The EEDRs are pointed by the black arrows

The comparison of the model results calculated with and without electromagnetic drift (1 and 2 correspondingly) shows that the electric field influences on locations of the EEDRs equatorial and high-latitudinal "sides" only. This can be explained in the following way: the EEDRs are bounded by the main ionospheric trough from poles and by the trough over the geomagnetic equator formed due to the night-time remains of the equatorial anomaly. The switching-off of the electromagnetic drift results in the decrease of both trough depths in the version (2) foF2 distribution. The steepness of the low- and high-latitudinal EEDRs "sides" decreases.

So the EEDRs are formed by the neutral wind action. In the night sector the equatorward neutral wind drives the F2-layer plasma to higher altitudes where the ion loss rate is lower. This mechanism acts jointly with plasma flows from the plasmasphere resulting in F2-region plasma density increasing. The ionosphere-plasmasphere exchange is taken into account in the UAM self-consistently by integrating $O^+$ and $H^+$ continuity equations along the geomagnetic field lines.

**4. Seasonal variation of the EEDRs**

We have calculated global 3D $n_e$ patterns for two quiet days representing December (23.12.1985) and June (23.06.1986) solstices under low solar activity level by using the following UAM configurations:

1) version with thermospheric parameters and 3D circulation calculations by solving the momentum, continuity and heat balance equations (marked as UAM-TT);

2) version with thermospheric parameters calculation using the empirical thermospheric NRLMSISE-00 model (*Picone et al.*, 2002) (marked as UAM-MSIS);

3) version with neutral composition and temperature calculation using the NRLMSISE-00 model and horizontal velocities of the thermospheric wind calculation using the empirical model HWM-93 (*Hedin et al.*, 1996) (marked as UAM-MSIS-HWM).

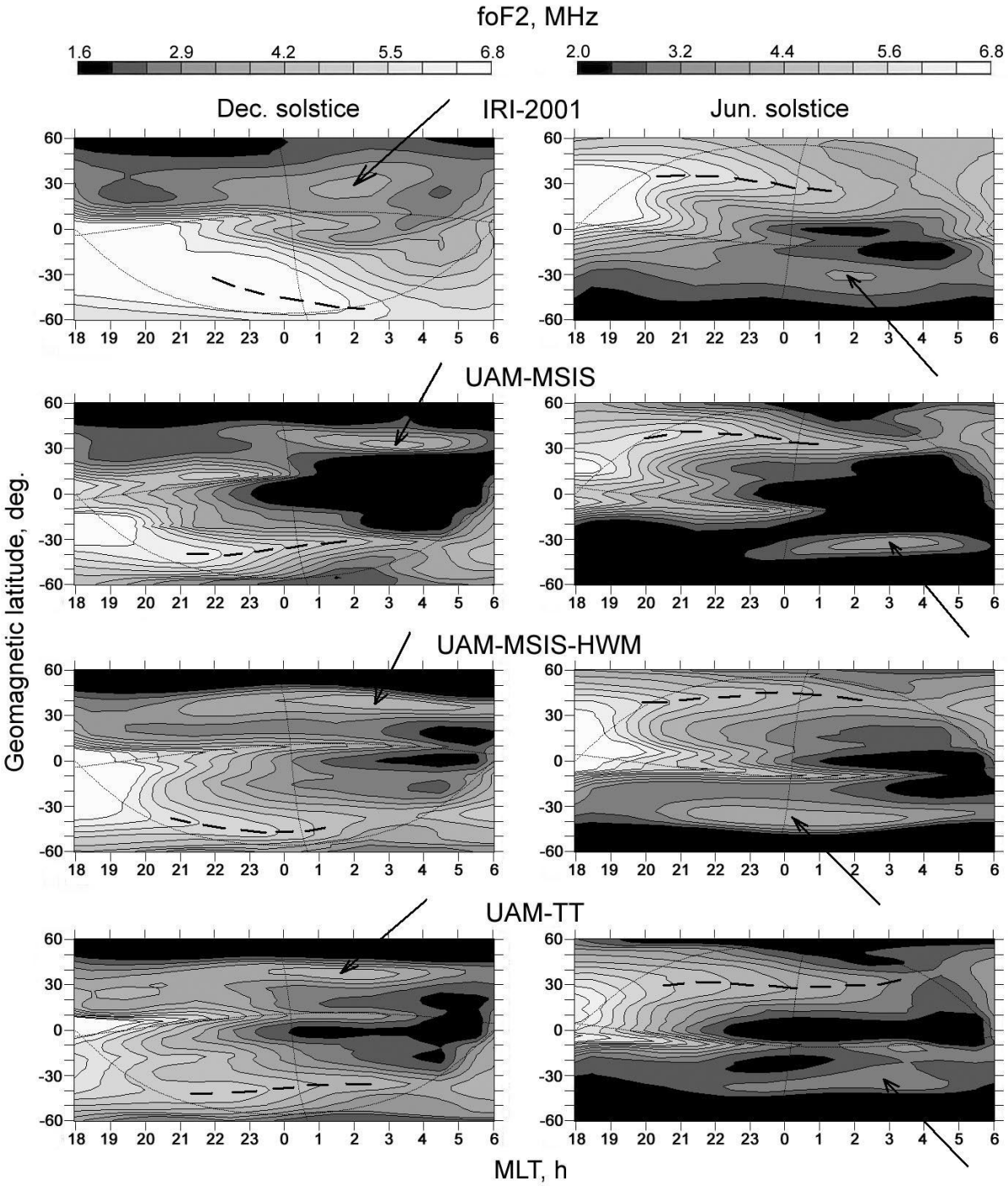


Fig. 2. Geomagnetic foF2 maps at the night longitudinal sector (18:00-06:00 MLT) calculated for the December solstice (23.12.1985) for 06:00 UT (left column) and for the June solstice (23.06.1986) for 18:00 UT (right column). At the first upper row the IRI-2001 results are presented; at the second one – of the UAM-MSIS version; at the third one – of the UAM-MSIS-HWM version; at the fourth one – of the UAM-TT version. The midday-midnight geodetic meridian, the terminator and geodetic equator are drawn by the dotted lines on the maps. The winter EEDRs type is pointed by the black arrows. The summer type is pointed by the dashed black lines

The numerical modeling results are compared with the IRI-2001 data.

The geomagnetic foF2 maps calculated by the UAM and IRI-2001 models at the night-time MLT sector are shown in Fig. 2 for the December solstice (left column) and the June one (right column) for fixed moments of 06 and 18 UT correspondingly. The maps format is the same as in the previous figure.

The EEDRs of two types are clearly visible in both geomagnetic hemispheres in the UAM calculation results: 1) the *winter type* with maxima at the latitudinal and diurnal NmF2 variations (pointed by the black arrows) and 2) the *summer type* with maximum at the latitudinal variation only (pointed by the black dashed lines).

The IRI-2001 model reproduces both types of the EEDRs but in its results these regions are less visible in the Southern Hemisphere than in the Northern one. Apparently this is explained that the number of the ionosonde stations is less in the Southern Hemisphere.

The amplitudes of foF2 enhancement in the EEDRs over the background values are larger in winter conditions than in the summer ones. It agrees with the experimental data (*Mikhailov et al.*, 2000; *Farelo et al.*, 2002).

All UAM versions differ by the method of the 3D thermospheric circulation calculation. It explains the differences of the EEDRs life-time, latitudinal location and amplitude of the foF2 enhancements caused by the corresponding longitudinal-latitudinal variations of the thermospheric wind at the night sector.

**5. Longitudinal variation of the EEDRs**

As the main cause of the EEDRs forming is the thermospheric wind pushing plasma along the geomagnetic field lines, these regions must depend on the UT moment (UT-effect) and the longitudinal sector due to the non-coincidence of the geomagnetic and geodetic axes.

Figs 3-4 present the results of the model calculations (the IRI-2001, the UAM-MSIS, the UAM-MSIS-HWM, the UAM-TT – from top to down in Fig.3-4) of the latitudinal-temporal foF2 variations for two geodetic meridians $\lambda_1 = 105°$ and $\lambda_2 = 285°$ under low solar activity for the December solstice (summer in the Southern Hemisphere) (Fig. 3) and the June solstice (summer in the Northern Hemisphere) (Fig. 4). Meridian $\lambda_2 = 285°$ passes across the Weddell Sea anomaly region. The geomagnetic equator is marked by the horizontal solid black line.

Fig. 3 shows that all UAM versions and IRI-2001 model reproduce night-time EEDRs summer type in the Southern Hemisphere at the geodetic meridian $\lambda_2 = 285°$ (marked by the solid black circles). These regions have a characteristic property: the summer night-time foF2 values in the EEDRs exceed the day-time foF2 values. Just this phenomenon is called the Weddell Sea anomaly (WSA). At the meridian $\lambda_1 = 105°$ the EEDRs are absent.

In the UAM the summer night-time densities in the WSA exceed the day-time ones by the same factor as in the IRI (IRI: factor of 1.2 for foF2 or 1.4 for NmF2, UAM: factor of 1.3 for foF2 or 1.7 for NmF2). But in comparison with the IRI model the UAM gives the WSA at lower geodetic latitudes (IRI: 48º-80ºS, UAM-MSIS: 44º-64ºS, UAM-MSIS-HWM: 42º-66ºS, UAM-TT: 40º-54ºS) and earlier by LT (IRI: ~20 to 2 LT, all UAM versions: 18 to 23 LT). We discuss these differences later (in Section Discussion).

For the June solstice in the Northern Hemisphere all model calculations show that the analogous WSA phenomenon is formed at the geodetic meridian $\lambda_1 = 105°$ in the summer Northern Hemisphere (Fig. 4, marked by the solid black lines) and it is absent at $\lambda_2 = 285°$.

Discussed model calculation results were obtained by using the UAM taking into account the non-coincident geodetic and geomagnetic axes. Both anomalies occur in summer hemispheres where the geomagnetic equator was located. Though these regions are projected at the subauroral geodetic latitudes, these are phenomena of the geomagnetic middle-latitude F2-layer.

As it was shown earlier the EEDRs are formed by the neutral wind action, particularly by the ion momentum transfer induced by the thermospheric wind along the geomagnetic field lines. The vertical ion velocity induced by the meridional wind (Fig. 5) is:

$$V_{iz} \sim V_{i||} \cdot \sin I \sim V_{nx} \cdot \cos I \cdot \sin I, \quad (6)$$

where $I$ – the inclination of the magnetic field $\boldsymbol{B}$, $\boldsymbol{V_{nx}}$ – the meridional velocity of the neutral particles in the magnetic meridian, $\boldsymbol{V_{i||}}$ – the projection of $\boldsymbol{V_{nx}}$ at the magnetic field line (field-aligned ion velocity received by collision with a neutral particle), $\boldsymbol{V_{iz}}$ – the projection of $\boldsymbol{V_{i||}}$ at the vertical direction (axis z). The vertical ion velocity $V_{iz}$ induced by the wind is proportional to the $\cos I \cdot \sin I$ value.

When the geomagnetic and geodetic axes are not coincident, the $\cos I \cdot \sin I$ magnitude at the fixed geodetic latitude depends on the geodetic longitude value. For example, Fig. 6 shows that the WSA locates at the longitudinal sector (255°-315°) for which the $\cos I \cdot \sin I$ has the maximal values.

**6. Discussion**

Now let us consider the plasmaspheric flux influence on the night-time ionospheric F2-layer behaviour. Fig. 7 shows the IRI and UAM modeled LT-variations of the NmF2, hmF2, $V_{nx}$ (h = 300 km), $T_e$ (h = 500 km) and $H^+$ flux (h = 1000 km) at 3 geodetic latitudes and 2 geodetic meridians both for the winter (Northern) and summer (Southern) Hemispheres. We can see the following peculiarities of these variations in this figure.

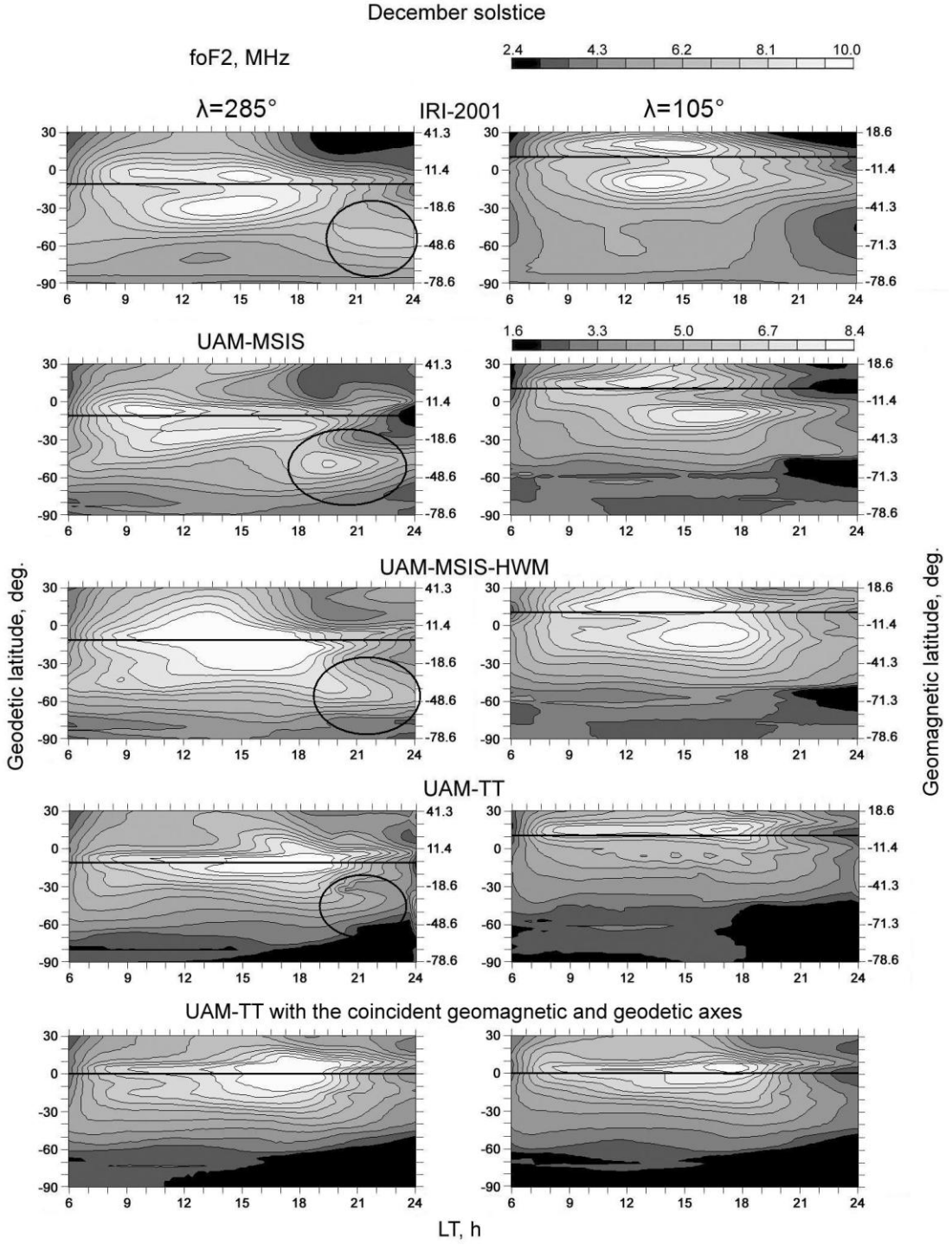


Fig. 3. Latitudinal-temporal foF2 variations in the summer Southern Hemisphere under low solar activity calculated for the December solstice (23.12.1985) for two geodetic meridians $\lambda_1 = 105°$ (right column) and $\lambda_2 = 285°$ (left column). At the first upper row the results of calculation by the IRI-2001 are presented; at the second one – by the UAM-MSIS version; at the third one – by the UAM-MSIS-HWM version; at the fourth one – by the UAM-TT. At the fifth row the results of calculation by the UAM-TT version with the coincident geomagnetic and geodetic axes are presented. The geomagnetic equator is marked by the horizontal solid black line. The Weddell Sea anomaly is marked by the solid black circles

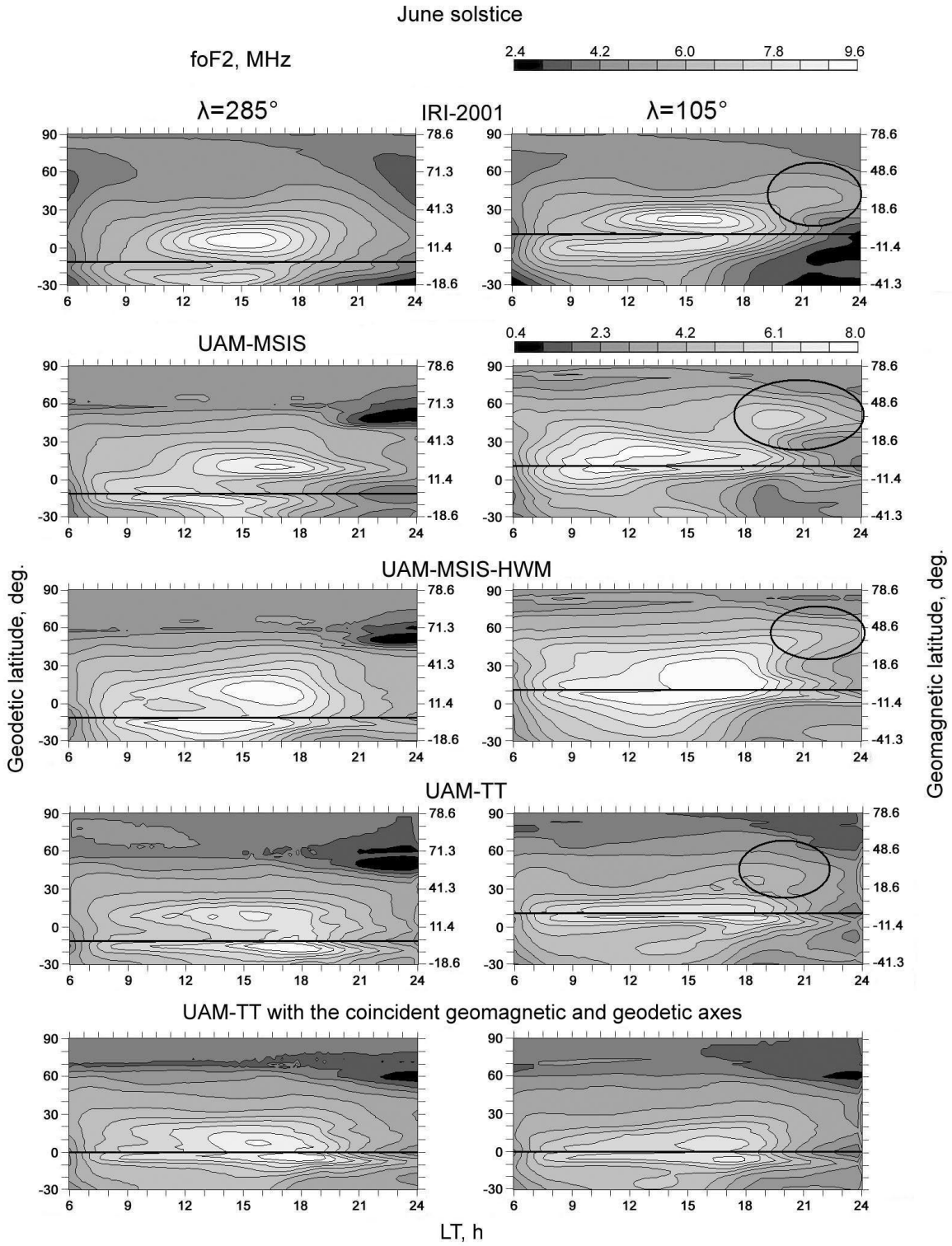


Fig. 4. Same as in Fig. 3, but for the June solstice (23.06.1986). The analogous WSA anomaly in the Northern summer Hemisphere is marked by the solid black circles

At 285 deg. long. meridian (close to Millstone Hill) IRI shows a weak NmF2 maximum near 03LT and a rather flat hmF2 of about 310 km. Both UAM versions show the more smooth NmF2(LT) than that by IRI with hmF2 of about 275-300 km and positive equatorward winds after 18LT till midnight when they reach 100-120 m/s then decreasing to zero. $H^+$ flux ($h$ = 1000 km) is close to zero between 18 and 06LT.

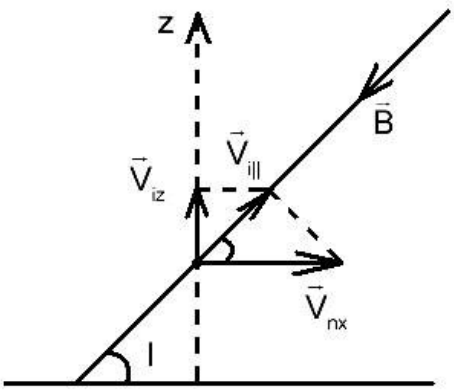


Fig. 5. Ion momentum transfer due to collision with a neutral particle along the geomagnetic field line

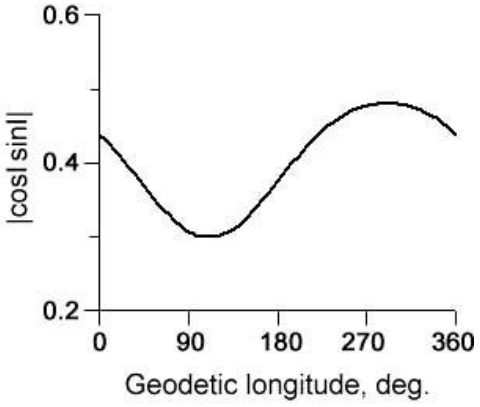


Fig. 6. Variation of |cos*I*·sin*I*| value at fixed geodetic latitude (45º S)

We should mention the peculiarity of the winter anomaly in the American sector which is related to the fact that in this sector middle geodetic latitudes belong to the subauroral geomagnetic latitudes. Millstone Hill is rather subauroral than mid-latitudinal station. Fast zonal drifts (polarization jets) are often observed here. Near midnight these drifts can diverge or converge depending on what electric fields (determined by FAC1 or FAC2) dominate there. It means that only three-dimensional consideration with a correct description of electric fields is required for this location.

At 105 deg. long. meridian IRI shows a pronounced NmF2 maximum near 01-02LT with hmF2 rather similar to that at 285 deg. longitude. Both UAM versions (TT and MSIS-HWM) give (show) the same NmF2 from 18 till 24LT reaching maximum near 23LT with hmF2 of about 250-275 km. Equatorward winds are negative till 20LT and remain close to zero in UAM-TT version after this time moment and small positive ($V_{nx}$<50m/s) between 20 and 23LT in UAM-MSIS-HWM version. $H^+$ fluxes are downwards directed at this time interval in both UAM versions. Therefore namely these fluxes are responsible for the pre-midnight NmF2 growth. After 23LT winds remain close to zero in UAM-TT version, $H^+$ fluxes decrease and NmF2 drops in this UAM version whereas in the UAM-MSIS-HWM versions positive equatorward winds continue to grow resulting in the growth of NmF2 and hmF2. Therefore namely winds are responsible for the forming of the second NmF2 maximum at 05LT in the UAM-MSIS-HWM version.

It is interesting that the UAM results overestimate the IRI values in the cases when the UAM overestimates downward H+ fluxes which support the ionospheric F2-layer. The last depends on the plasmaspheric tube fullness. When the UAM versions have the same plasmaspheric fluxes and winds, their electron density values are very close to each other too.

At 285 deg. longitude IRI shows a maximum of NmF2 at 22LT at 45-50 deg. latitudes with the HmF2 maximum of about 350 km approximately at the same time. Both UAM versions give NmF2 maximum at 20LT with lower electron density values in the UAM-TT version. $H^+$ fluxes are upwards directed in both UAM versions from 16 till 21LT (being more intensive in the UAM-TT version) then reversing their directions in the UAM-TT version and remaining near zero in the UAM-MSIS-HWM version. Equatorward winds have two approximately equal maxima at 22 and 02 LT in the UAM-TT version producing analogous hmF2 variation. In the UAM-MSIS-HWM version the second maximum of the winds dominates but this does not reflect in the hmF2 (LT) variation. We see that NmF2 in the UAM-MSIS-HWM version drops too fast after its maximum due to lack of the support by the plasmaspheric fluxes and insufficiently high equatorward wind velocities. In the UAM-TT version NmF2 drops more slowly after its maximum but the NmF2 values are lower due to the low sunset values.

Fig. 7, summer 285E provides an explanation for the displacement of the WSA density maximum from 22 LT in the IRI to 20 LT in the UAM. Fig. 7 shows that the plasmaspheric fluxes were upward-directed at 16-21 LT and 03-08 LT. For 21-03 LT the UAM gives the downward fluxes but their values were too small and not sufficient to support the ionospheric F2-layer density. To increase the plasmaspheric downward flux, we should use more fulfilled initial state of the plasmasphere. But in this case we obtain too large exceeding of the UAM density over the IRI one at winter 105ºE. Besides, as we can see from Fig. 7, the hmF2 values of both UAM versions at summer 285E underestimate the IRI results. It means that both the UAM and the HWM winds at this location are insufficient in comparison with real winds determining the peak electron density level. Therefore, the displacement of the density maximum from 22 LT in the IRI to 20 LT in the UAM is caused by too low both winds and fluxes at this location after 20 LT.

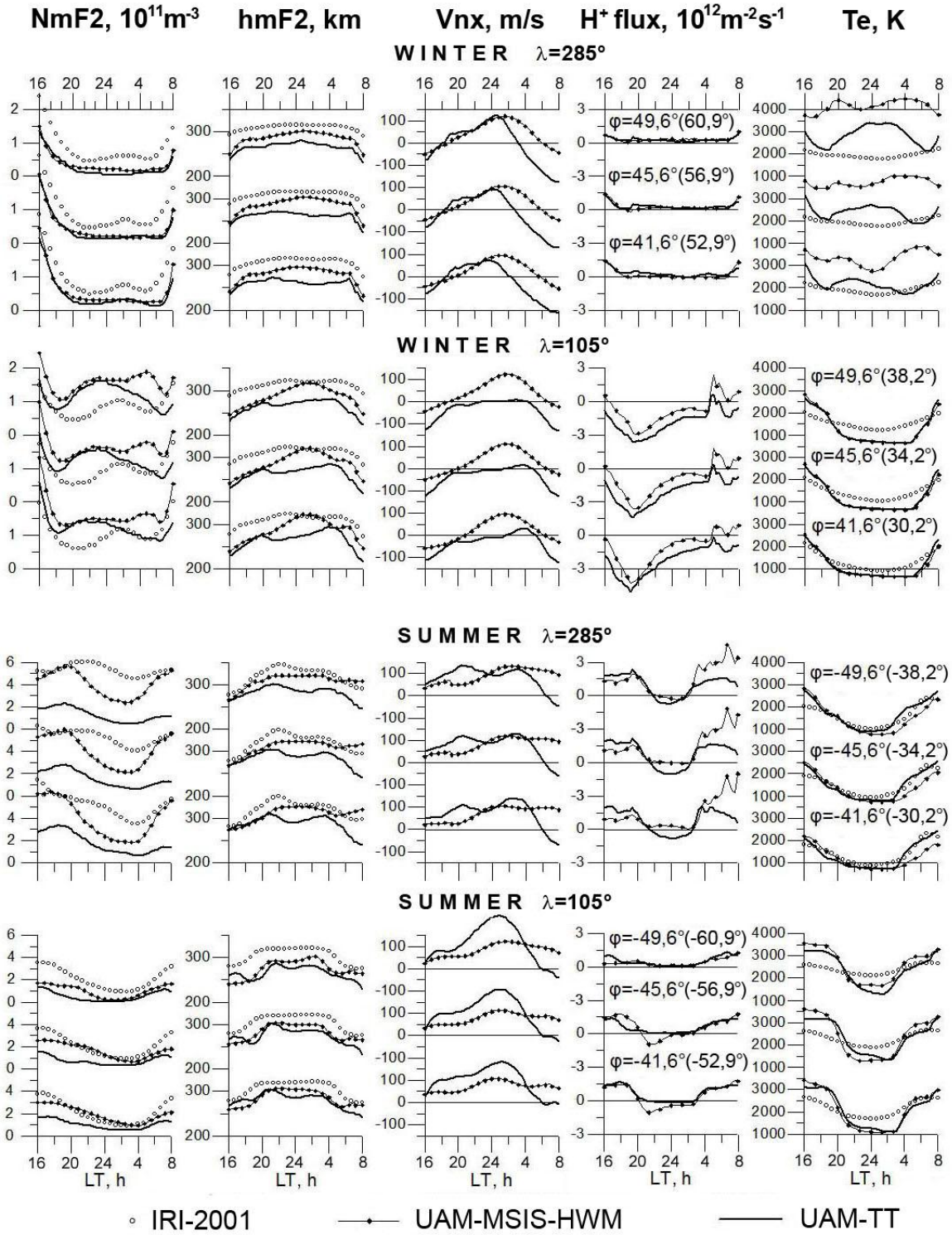


Fig. 7. LT-variations of the NmF2, hmF2, $V_{nx}$ (h = 300 km), $T_e$ (h = 500 km) and $H^+$ flux (h = 1000 km) calculated by the IRI and UAM (MSIS-HWM and TT) at 6 geodetic latitudes (φ=±49.6°, ±45.6° and ±41.6°) and 2 geodetic meridians ($\lambda$ = 285° and 105°) both for the winter (Northern) and summer (Southern) Hemispheres. The $V_{nx}$ positive values correspond to equatorward meridional wind. The upward $H^+$ fluxes are positive. Corresponding geomagnetic latitudes are in brackets

At 105 deg. longitude nor IRI neither UAM show any nighttime summer NmF2 enhancements. The UAM-MSIS-HWM NmF2 agree better with IRI (sometimes coinciding) than UAM-TT but HmF2 in IRI (of about 325 km) are higher than in UAM (275-300 km). More high wind velocities are required therefore in the pre-

midnight hours to improve the agreement between both NmF2 and hmF2 values calculated by IRI and UAM.

It is evident that the IRI-UAM agreement can be improved by initial conditions calibration, particularly by correct setting of plasma tubes fullness. It means that plasmaspheric initial conditions by the UAM simulations are to be longitude dependent. This implies different tubes fullness at different geomagnetic meridians. Such initial condition setting is inappropriate because firstly it is very laborious method and secondly an improvement of results agreement at some meridians will be accompanied by its deterioration at other meridians.

At last let us consider the electron temperature LT variations (last column in the figure). We see a rather good agreement between the IRI and UAM Te(LT) variations except the winter 285 deg. longitude where the UAM nighttime Te are higher than those of IRI. No signatures of the electron temperature influence on the nighttime F2-layer electron density enhancements are seen in the model calculation results.

Thus we conclude that the main cause of the WSA and analogous phenomenon in the Northern Hemisphere is the non-coincidence of the geodetic and geomagnetic axes. Due to this non-coincidence the ion momentum transfer along the geomagnetic field lines by the thermospheric wind forms the longitudinal electron density variations with the anomalous diurnal variation in the Southern and Northern Hemispheres under summer condition.

In order to check this we calculated the electron density variations in the same longitudes without taking into account the non-coincidence of the geodetic and geomagnetic axes. The results of corresponding UAM calculations are presented in Figs 3-4 (bottom panels). The figures show that in this case the WSA and analogous phenomenon in the Northern Hemisphere practically disappeared. We suggest that the whole disappearance of the phenomenon can be reached by the exception of the initial conditions influence on the model results.

**7. Conclusion**

Thus the analysis of the results of the model calculations ionospheric F2-layer electron density by using the global numerical model of the Earth's upper atmosphere and the empirical model of the ionosphere IRI-2001 results in the following conclusions.

1) The main cause of the occurrence of the night-time middle-latitude enhanced electron density regions is the joint action of the equatorward thermospheric wind and the plasma flows from the plasmasphere to the night-time ionosphere.

2) The electric field influences only on the latitudinal location of the equatorial and high-latitudinal EEDRs "sides" by forming the main ionospheric trough at the high latitudes and the trough over the geomagnetic equator.

3) The seasonal EEDRs variations are expressed by the existence of two types of these regions: 1) winter type with maxima in the latitudinal and diurnal foF2 variations and 2) summer type with the maximum in the latitudinal variation only. Both EEDRs types formation is caused by the corresponding season variations of the thermospheric wind.

4) The Weddell Sea Anomaly in the Southern Hemisphere and the analogous longitudinal variation in the Northern Hemisphere under the summer conditions are the summer type of the EEDRs. The numerical experiments have shown that both phenomena are caused by the non-coincidence of the geomagnetic and geodetic axes which produces the difference in vertical velocities of the ion transfer by the thermospheric wind action at different longitudinal sectors.

5) The UAM-IRI comparison shows that the empirical and theoretical models reproduce rather similar global electron density patterns with EEDRs of both winter and summer types with the same levels in magnitude but with differences (of about 2-4 hours) in local time of occurrences. Such displacement in LT can be related with the simplified geomagnetic field model and inaccuracies in neutral wind velocity and plasmasphere-ionosphere fluxes calculations in the UAM.

**References**

**Bailey G.L., Sellek R., Balan N.** The effect of interhemispheric coupling on nighttime enhancements in ionospheric total electron content during winter at solar minimum. *Annales Geophysicae*, v.9, N 11, p.738-747, 1991.

**Balan N., Bailey G.J., Nair R.B.** Solar and magnetic activity effects on the latitudinal variations of nighttime TEC enhancement. *Annales Geophysicae*, v.9, N 1, p.60-69, 1991.

**Balan N., Rao P.B.** Latitudinal variations of nighttime enhancements in total electron content. *Journal of Geophysical Research*, v.92, N A4, p.3436-3440, 1987.

**Balan N.P., Rao P.B., Iyer K.N.** Seasonal and solar cycle variations of nighttime anomalous enhancements in total electron content. *Proceedings of Indian Academy of Sciences, Earth Planetary Science*, v.95, p.409-416, 1986.

**Bellchambers W.H., Piggott W.R.** Ionospheric measurements made at Halley Bay. *Nature*, v.182, p.1596-1597, doi:10.1038/1821596a0, 1958.

**Bertin F., Lepine J.P.** Latitudinal variation of total electron content in the winter at middle latitudes. *Radio Science*, v.5, N 6, p.899-906, 1970.

**Bilitza D.** International reference ionosphere 2000. *Radio Science*, v.36, N 2, p.261-275, 2001.

**Brunelli B.E., Namgaladze A.A.** Physics of the ionosphere. *M., Nauka*, 528 p., 1988.

**Brunini C., Van Zele M.A., Meza A., Gende M.** Quiet and perturbed ionospheric representation according to the electron content from GPS signals. *Journal of Geophysical Research*, v.108, N A2, doi:10.1029/2002JA009346, 2003.

**Burns A.G., Zeng Z., Wang W., Lei J., Solomon S.C., Richmond A.D., Killeen T.L., Kuo Y.-H.** Behavior of the F2 peak ionosphere over the South Pacific at dusk during quiet summer conditions from COSMIC data. *Journal of Geophysical Research*, v.113, eid:A12305, doi:10.1029/2008JA013308, 2008.

**Da Rosa F.V., Smith F.L.** Behaviour of the night-time ionosphere. *Journal of Geophysical Research*, v.72, N 7, p.1829-1836, 1967.

**Davies K., Anderson D.N., Paul A.K., Degenhardt W., Hartmann G.K., Leitinger R.** Nighttime increases in total electron content observed with the ATS 6 radio beacon. *Journal of Geophysical Research*, v.84, N A4, p.1536-1542, 1979.

**Davies K., Hartmann G.K.** Studying the ionosphere with the Global Positioning System. *Radio Science*, v.32, N 4, p.1695-1703, 1997.

**Dudeney J.R., Piggott W.R.** Antarctic ionospheric research, in Upper Atmosphere Research in Antarctica. *Antarctic Research Series*, v.29, p.200-235, 1978.

**Evans J.V.** Cause of the midlatitude winter night increase in foF2. *Journal of Geophysical Research*, v.70, N 17, p.4331-4345, 1965.

**Farelo A.F., Herraiz M., Mikhailov A.V.** Global morphology of night-time NmF2 enhancements. *Annales Geophysicae*, v.20, N 11, p.1795-1806, 2002.

**Förster M., Jakowski N.** The nighttime winter anomaly (NWA) effect in the American sector as a consequence of interhemispheric ionospheric coupling. *PAGEOPH*, v.127, N 2, p.447-471, 1988.

**Garner T.W., Richards P.G., Comfort R.H.** Anomalous nighttime electron temperature events over Millstone Hill. *Journal of Geophysical Research*, v.99, N A6, p.11.411-11.415, doi:10.1029/94JA00261, 1994.

**Gilliland T.R.** Multifrequency ionosphere recording and its significance. *Proceedings of the Institute of Radio Engineers*, v.23, p.1076, 1935.

**He M., Liu L., Wan W., Ning B., Zhao B., Wen J., Yue X., Le H.** A study of the Weddell Sea Anomaly observed by FORMOSAT-3/COSMIC. *Journal of Geophysical Research*, v.114, eid:A12309, doi:10.1029/2009JA014175, 2009.

**Hedin A.E., Fleming E.L., Manson A.H., Schmidlin F.J., Avery S.K., Clark R.R., Franks S.J., Fraser G.J., Tsuda T., Vial F., Vincent R.A.** Empirical wind model for the upper, middle and lower atmosphere. *Journal of Atmospheric and Terrestrial Physics*, v.58, N 13, p.1421-1447, 1996.

**Ho C.M., Mannucci A.J., Lindqwister U.J., Pi X., Tsurutani B.T.** Global ionosphere perturbations monitored by the worldwide GPS network. *Geophysical Research Letters*, v.23, N 22, p.3219-3222, 1996.

**Ho C.M., Mannucci A.J., Sparks L., Pi X., Lindqwister U.J., Wilson B.D., Iijima B.A., Reyes M.J.** Ionospheric total electron content perturbations monitored by the GPS global network during two Northern Hemisphere winter storms. *Journal of Geophysical Research*, v.103, N A11, p.26.409-26.420, 1998.

**Horvath I.** A total electron content space weather study of the nighttime Weddell Sea Anomaly of 1996/1997 southern summer with TOPEX/Poseidon radar altimetry. *Journal of Geophysical Research*, v.111, eid:A12317, doi:10.1029/2006JA011679, 2006.

**Horvath I., Essex E.A.** Using observations from the GPS and TOPEX satellites to investigate night-time TEC enhancements at mid-latitudes in the Southern Hemisphere during a low sunspot number period. *Journal of Atmospheric and Solar-Terrestrial Physics*, v.62, N 5, p.371-391, 2000.

**Horvath I., Essex E.A.** The Weddell Sea Anomaly observed with the TOPEX satellite data. *Journal of Atmospheric and Solar-Terrestrial Physics*, v.65, p.693-706, 2003.

**Horvath I., Lovell B.C.** An investigation of the Northern Hemisphere midlatitude nighttime plasma density enhancements and their relations to the midlatitude nighttime trough during summer. *Journal of Geophysical Research*, v.114, eid:A08308, doi:10.1029/2009JA014094, 2009a.

**Horvath I., Lovell B.C.** Distinctive plasma density features of the topside ionosphere and their electrodynamics investigated during southern winter. *Journal of Geophysical Research*, v.114, A01304, doi:10.1029/2009JA013683, 2009b.

**Horvath I., Lovell B.C.** Investigating the relationships among the South Atlantic Magnetic Anomaly, southern nighttime midlatitude trough, and nighttime Weddell Sea Anomaly during southern summer. *Journal of Geophysical Research*, v.114, eid:A02306, doi:10.1029/2008JA013719, 2009c.

**Horvath I., Lovell B.C.** Investigation of the southern daytime midlatitude trough's relation with the daytime Weddell Sea Anomaly during equinoxes. *Journal of Geophysical Research*, v.115, eid:A01302, doi:10.1029/2008JA014002, 2010.

**Jakowski N., Förster M.** About the nature of the nighttime winter anomaly effect (NWA) in the F-region of the ionosphere. *Planetary and Space Science*, v.43, N 5, p.603-612, 1995.

**Jakowski N., Jungstand A., Lois L., Lazo B.** Nighttime enhancement of the F2-layer ionization over Havana, Cuba. *Journal of Atmospheric and Terrestrial Physics*, v.53, N 11-12, p.1131-1138, 1991.

**Jee G., Burns A.G., Kirn Y.-H., Wang W.** Seasonal and solar activity variations of the Weddell Sea Anomaly observed in the TOPEX total electron content measurements. *Journal of Geophysical Research*, v.114, eid:A04307, doi: 10.1029/2008JA013801, 2009.

**Joshi H.P., Iyer K.N.** On nighttime anomalous enhancement in ionospheric electron content at lower mid-latitude during solar maximum. *Annales Geophysicae*, v.8, N 1, p.53-58, 1990.

**Karpachev A.T., Gasilov N.A., Karpachev O.A.** Reasons of the diurnal NmF2 variations at the middle- and subauroral latitudes under summer night-time conditions. *Geomagnetism and Aeronomy*, v.50, N 4, p.1-7, 2010.

**Klobuchar J.A., Aarons J., Hajeb Hosseinieh H.** Midlatitude nighttime total electron behavior during magnetically disturbed periods. *Journal of Geophysical Research*, v.73, N 23, p.7530-7534, 1968.

**Lin C.H., Liu J.Y., Cheng C.Z., Chen C.H., Liu C.H., Wang W., Burns A.G., Lei J.** Three-dimensional ionospheric electron density structure of the Weddell Sea Anomaly. *Journal of Geophysical Research*, v.114, eid:A02312, doi:10.1029/2008JA013455, 2009.

**Liu H., Thampi S.V., Yamamoto M.** Phase reversal of the diurnal cycle in the midlatitude ionosphere. *Journal of Geophysical Research*, v.115, eid:A01305, doi:10.1029/2009JA014689, 2010.

**Mikhailov A.V., Leschinskaya T.Yu., Förster M.** Morphology of NmF2 nighttime increases in the Eurasian sector. *Annales Geophysicae*, v.18, N 6, p.618-628, 2000.

**Namgaladze A.A., Korenkov Yu.N., Klimenko V.V., Karpov I.V., Bessarab F.S., Surotkin V.A., Glushchenko T.A., Naumova N.M.** Global model of the thermosphere-ionosphere-protonosphere system. *Pure and Applied Geophysics*, v.127, N 2/3, p.219-254, 1988.

**Namgaladze A.A., Korenkov Yu.N., Klimenko V.V., Karpov I.V., Surotkin V.A., Naumova N.M.** Numerical modelling of the thermosphere-ionosphere-protonosphere system. *Journal of Atmospheric and Solar-Terrestrial Physics*, v.53, N 11/12, p.1113-1124, 1991.

**Namgaladze A.A., Martynenko O.V., Namgaladze A.N.** Global model of the upper atmosphere with variable latitudinal integration step. *Geomagnetism and Aeronomy International*, v.1, N 1, p.53-58, 1998.

**Park C.G.** Westward electric fields as the cause of nighttime enhancements in electron concentrations in midlatitude F region. *Journal of Geophysical Research*, v.76, N 19, p.4560-4568, 1971.

**Pavlov A.V., Pavlova N.M.** Mechanism of the post-midnight winter night-time enhancements in NmF2 over Millstone Hill during 14-17 January 1986. *Journal of Atmospheric and Solar-Terrestrial Physics*, v.67, N 4, p.381-395, 2005.

**Pavlov A.V., Pavlova N.M.** Anomalous night-time peaks in diurnal variations of NmF2 close to the geomagnetic equator: A statistical study. *Journal of Atmospheric and Solar-Terrestrial Physics*, v.69, N 15, p.1871-1883, 2007.

**Penndorf R.** The average ionospheric conditions over the Antartic in Geomagnetism and Aeronomy. *Antartic Research Series*, v.4, p.1-45, 1965.

**Picone J.M., Hedin A.E., Drob D.P., Aikin A.C.** NRLMSISE-00 empirical model of the atmosphere: Statistical comparisons and scientific issues. *Journal of Geophysical Research*, v.107, N A12, doi:10.1029/2002JA009430, 2002.

**Rao M.M., Raj P.E., Joguly C.** A study of the post-sunset increase in the F2-region electron density at low- and middle latitudes in the Asian zone during sunspot maximum and minimum periods. *Annales Geophysicae*, v.38, N 3, p.357-365, 1982.

**Richards P.G., Buonsanto M.J., Reinisch B.W., Holt J., Fennelly J.A., Scali J.L., Comfort R.H., Germany G.A., Spann J., Brittnacher M., Fok M.-C.** On the relative importance of convection and temperature to the behavior of the ionosphere in North America during January 6-12, 1997. *Journal of Geophysical Research*, v.105, N A6, p.12.763-12.776, 2000.

**Richards P.G., Torr D.G., Reinisch B.W., Gamache R.R., Wilkinson P.J.** F2 peak electron density at Millstone Hill and Hobart: Comparison of theory and measurement at solar maximum. *Journal of Geophysical Research*, v.99, N A8, p.15.005-15.016, 1994.

**Thampi S.V., Lin C., Liu H., Yamamoto M.** First tomographic observations of the Midlatitude Summer Nighttime Anomaly over Japan. *Journal of Geophysical Research*, v.114, eid:A10318, doi:10.1029/2009JA014439, 2009.

**Titheridge J.E.** Nighttime changes in the electron content of the ionosphere. *Journal of Geophysical Research*, v.73, N 9, p.2985-2994, 1968.

**Titheridge J.E.** The electron content of the southern mid-latitude ionosphere, 1965-1971. *Journal of Atmospheric and Terrestrial Physics*, v.35, N 5, p.981-1001, 1973.

**Weimer D.R., Maynard N.C., Burke W.J., Liebrecht C.** Polar cap potentials and the auroral electrojet indicies. *Planetary and Space Science*, v.38, N 9, p.1207-1222, 1990.

**Wilson B.D., Mannucci A.J., Edwards C.D.** Subdaily Northern Hemisphere ionospheric maps using an extensive network of GPS receivers. *Radio Science*, v.30, N 3, p.639-648, 1995.

**Young D.M.L., Yuen P.C., Roelofs T.H.** Anomalous nighttime increases in total electron content. *Planetary and Space Science*, v.18, N 8, p.1163-1179, 1970.